Journal of ELECTRONIC MATERIALS, Vol. 45, No. 12, 2016
DOI: 10.1007/s11664-016-5033-0
© 2016 The Minerals, Metals & Materials Society

CrossMark

Influence of Carbon in Metalorganic Chemical Vapor Deposition of Few-Layer WSe_2 Thin Films

XIAOTIAN ZHANG,[1] ZAKARIA Y. AL BALUSHI,[1] FU ZHANG,[1] TANUSHREE H. CHOUDHURY,[1] SARAH M. EICHFELD,[1,2] NASIM ALEM,[1,2] THOMAS N. JACKSON,[1,3] JOSHUA A. ROBINSON,[1,2] and JOAN M. REDWING[1,2,3,4]

1.—Department of Materials Science and Engineering, The Pennsylvania State University, University Park, PA 16802, USA. 2.—Center for 2-Dimensional and Layered Materials, Materials Research Institute, The Pennsylvania State University, University Park, PA 16802, USA. 3.—Department of Electrical Engineering, The Pennsylvania State University, University Park, PA 16802, USA. 4.—e-mail: jmr31@psu.edu

Metalorganic chemical vapor deposition (MOCVD) is a promising technique to form large-area, uniform films of monolayer or few-layer transition metal dichalcogenide (TMD) thin films; however, unintentional carbon incorporation is a concern. In this work, we report the presence of a defective graphene layer that forms simultaneously during MOCVD growth of tungsten diselenide (WSe_2) on sapphire at high growth temperature and high Se:W ratio when using tungsten hexacarbonyl ($W(CO)_6$) and dimethyl selenide ($(CH_3)_2Se$, DMSe) as precursors. The graphene layer alters the surface energy of the substrate reducing the lateral growth and coalescence of WSe_2 domains. The use of hydrogen selenide (H_2Se) instead of DMSe eliminates the defective graphene layer enabling coalesced monolayer and few-layer WSe_2 films.

Key words: Metalorganic chemical vapor deposition (MOCVD), thin film, tungsten diselenide (WSe_2), transition-metal dichalcogenide, two-dimensional (2D) materials, carbon, dimethyl selenide, hydrogen selenide

INTRODUCTION

Since the discovery of graphene, layered materials, particularly transition metal dichalcognides (TMDs), have been reinvestigated in monolayer and few-layer form due to their unique properties such as tunable bandgap,[1] layer-dependent direct-to-indirect bandgap,[1] gate tunable superconductivity,[2,3] and mechanical flexibility.[4,5] Various synthesis processes have been developed to prepare TMD films including mechanical and chemical exfoliation,[6] metal transformation,[7,8] powder vaporization,[9,10] and chemical vapor deposition (CVD)/metalorganic CVD (MOCVD).[11,12] Of these methods, CVD/MOCVD stands out for its precise precursor controllability, scalability to large area substrates, and ability to fabricate heterostructures in situ through switching of source gases. Initial studies demonstrated the CVD and MOCVD growth of layered TMD films such as MoS_2 and WSe_2, hundreds of nanometers thick, using a variety of metal precursors ($W(CO)_6$, $Mo(CO)_6$, $MoCl_5$, WCl_6, etc.), and chalcogen sources (H_2S, $HSC(CH_3)_3$, diethyl selenide, etc.).[13–17] More recently, efforts have focused on adapting these processes for the synthesis of monolayer and few-layer films of TMDs such as MoS_2 and WS_2[11] and WSe_2.[12]

Unintentional carbon incorporation has been a persistent problem in MOCVD processes due to the use of precursor molecules with organic ligands. In the conventional MOCVD growth of III-V compound semiconductor thin films, carbon concentrations are typically lower than 10^{15} cm^{-3}.[18] However, even low levels of carbon can impact device performance and, therefore, carbon as both an unintentional impurity

(Received August 25, 2016; accepted October 6, 2016; published online October 20, 2016)

and intentional dopant in MOCVD has been thoroughly investigated over the years. Compared to conventional MOCVD-grown semiconductor layers, which may be hundreds of nanometers or more in thickness, two-dimensional (2D) TMD monolayers are atomically thin with highly reactive edge surfaces and are bound to the substrate by van der Waals forces. Therefore, the presence of even small amounts of carbon in TMD growth may impact the nucleation and lateral growth of TMD layers and the resulting structural, optical and electrical properties of the films.

In the case of WSe_2, previous studies have demonstrated that MOCVD growth conditions, particularly substrate temperature and selenium-to-tungsten (Se:W) ratio, play a significant role in the nucleation and lateral growth of the films.[12] The high melting temperature/low vapor pressure of transition metals such as W results in reduced surface adatom mobility which necessitates the use of high substrate temperatures ($>600°C$) to enhance surface diffusion and achieve large domain sizes. On the other hand, the low melting temperature/high vapor pressure of Se and other chalcogens reduces the sticking coefficient of Se on the growth surface which makes it necessary to use very high Se:W ratios in order to achieve stoichiometric films. Although the presence of residual carbon was noted in TMD monolayer and few-layer thin films grown using MOCVD precursors,[11,12] it has not been investigated in detail.

In this study, we examined the growth of WSe_2 thin films on (0001) sapphire substrates by MOCVD in a vertical cold-wall reactor chamber using tungsten hexacarbonyl ($W(CO)_6$), dimethyl selenide ($(CH_3)_2Se$, DMSe), and hydrogen selenide (H_2Se) as precursors. The studies reveal the formation of a defective graphene layer on the sapphire substrate at high substrate temperature ($\sim800°C$) and Se/W ratios over 3200 when DMSe is used as the Se precursor, which impacts the nucleation and growth of WSe_2. Carbon deposition does not occur when H_2Se is used in place of DMSe indicating that the methyl radicals from DMSe are the primary source of carbon. The results suggest that the carbon layer formation competes with the nucleation and growth of WSe_2 on the sapphire surface and impacts the lateral and vertical growth of the triangular WSe_2 islands.

EXPERIMENTAL PROCEDURE

Tungsten diselenide films were synthesized using tungsten hexacarbonyl (Sigma-Aldrich, 99.99% purity), dimethyl selenide (NOVA-KEM, 99.99% purity), and hydrogen selenide (Matheson, 99.998% purity) in a cold-wall vertical quartz tube reactor with an inductively heated SiC-coated graphite susceptor. Ultra-high purity hydrogen was used as the carrier gas through the bubblers and reactor to maintain a total flow rate at 450 sccm. The $W(CO)_6$ powder was contained inside a stainless steel bubbler, which was held at 30°C and 97 kPa. Hydrogen carrier gas was passed through the bubbler at a flow rate of 15 sccm which resulted in a $W(CO)_6$ flow rate of 9×10^{-4} sccm out of the bubbler. DMSe liquid was also contained inside a stainless steel bubbler, which was held at room temperature and 101 kPa. Hydrogen carrier gas was passed through the bubbler at a flow rate in the range of 2.5–25 sccm, which resulted in a DMSe flow rate of 0.75–7.5 sccm out of the bubbler. Growth was carried out at a total reactor pressure of 93 kPa, a growth time of 30 min and a substrate temperature of 800°C for all experiments. As-received c-plane (001) double-side polished sapphire (Cryscore Optoelectronic Ltd, 99.996% purity, Ra roughness <0.2 nm) were used as substrates. The sapphire substrates were cleaned through rinsing with acetone, 2-propanol and deionized water, then drying with nitrogen.

Elemental compositions of different regions on the sample surface were analyzed by high resolution Auger electron spectroscopy (AES) in a PHI 720 Scanning Auger Nanoprobe using 10 keV electron beam energy. Raman spectroscopy was carried out in a HORIBA LabRAM HR Evolution high spectral resolution analytical Raman microscope with a laser wavelength of 532 nm. To measure the film thickness and domain heights, a step edge was formed on the as-grown WSe_2 film via using a plastic tweezer to scratch the sample surface and the step height was profiled using a Digital Instruments Multimode Atomic Force Microscope (AFM). Field emission scanning electron microscopy (FESEM) images were obtained in a Zeiss Merlin instrument. Transmission electron microscopy (TEM) was used to examine the cross-sectional morphology and obtain structural information on the WSe_2 samples. Cross-sectional TEM samples were fabricated by the focused ion beam (FIB) method on a HELIOS Nanolab 660. A thin layer of gold was sputtered on top of the substrate to enhance the conductivity. A layer of platinum was deposited to protect and mark the cut region. A FEI Tecnai G2 TEM operating at 80 kV was used to study the atomic structure of the WSe_2 samples produced in this study.

RESULTS AND DISCUSSION

The effect of Se:W ratio on the nucleation and lateral growth of WSe_2 on sapphire was initially investigated by maintaining a constant $W(CO)_6$ partial pressure of 1.9×10^{-4} kPa in the reactor chamber and varying the flow rate of DMSe to change the Se:W ratio from approximately 800 to 8000. The WSe_2 domain size increased and the nucleation density decreased as the Se:W ratio was increased from 800 to 4800, as shown in Fig. 1a–d. Further increases in the Se:W ratio up to 8000 did not result in a significant increase in the domain size or a reduction in the nucleation density (surface coverage), as shown in Fig. 1e and f. Interestingly,

while the surface coverage of WSe_2 domains was reduced at high Se:W ratios above 3200, the height of the domains increased significantly from ~10 nm at Se:W = 3200 to 20–30 nm for Se:W ratios ranging from 4800 to 8000 (Fig. 1g). In addition, as the Se:W ratio was increased above 3200, the edges of the triangular domains become jagged and pits appear in the islands and near the domain edges (Fig. 1d). Prior studies have reported changes in the shape and edge structure of TMD domains as a function of the chalcogen-to-metal ratio[19] and growth rate[20] and in the presence of impurities and oxidation[21] and intentional dopants.[22]

The change in the lateral versus vertical growth rate at high Se:W ratios as well as the deformed edge shape suggests changes in surface energy, which make it more energetically favorable for the WSe_2 to grow vertically on existing domains instead of laterally on the substrate surface. When examining the scratched sample surface that was used to obtain a step height for domain thickness measurements by FESEM (Fig. 2a), a region of darker contrast (region 3) was observed between the WSe_2 triangle domains (region 2) and the sapphire surface (region 1) at the scratched boundary, which suggested the presence of a thin layer of different conductivity on the surface. This layer was determined to be ~1.5 nm thick from AFM measurements (Fig. 2b). AES was used to analyze the elemental composition of the three regions with different FESEM contrasts, as shown in Fig. 2c. Only Al and O were detected on the sapphire surface region (region 1). As expected, W and Se elements were detected in the triangular domain regions (region 2) consistent with the formation of WSe_2 along with a small carbon signal. In the region between the WSe_2 domains (region 3); however, a strong carbon signal was observed but no W or Se signals indicating that the thin layer on the sapphire surface contains mostly carbon. A cross-sectional TEM image of the sample grown using DMSe at 800°C and Se:W = 3200, shown in Fig. 3, obtained in an area similar to that of region 2 above, revealed a carbon layer beneath the WSe_2 domains. The thickness of this carbon layer is ~2 nm, which is consistent with the AFM thickness measurement in Fig. 2b. Additional cross-sectional TEM images obtained from different regions across the sample show that the thickness of the carbon layer varies from ~1.2 nm to ~5.5 nm. The WSe_2 layer is ~6 nm thick and shows a layered structure with spacing between layers of ~0.67 nm which is consistent with WSe_2. Some regions of the carbon layer exhibit a layered structure indicating the formation of graphene.

The carbon layer present in the WSe_2 sample shown in Figs. 2 and 3 likely results from the high concentration of carbon-containing ligands present in the MOCVD growth environment. Prior studies have demonstrated that methane (CH_4) can be used as a precursor to deposit graphene on sapphire at temperatures as low as 950°C.[23,24] Graphene produced by this process is typically defective as demonstrated by the presence of a strong D peak at ~1350 cm^{-1} in the Raman spectra.[23,25,26] The methyl radicals produced by the decomposition of

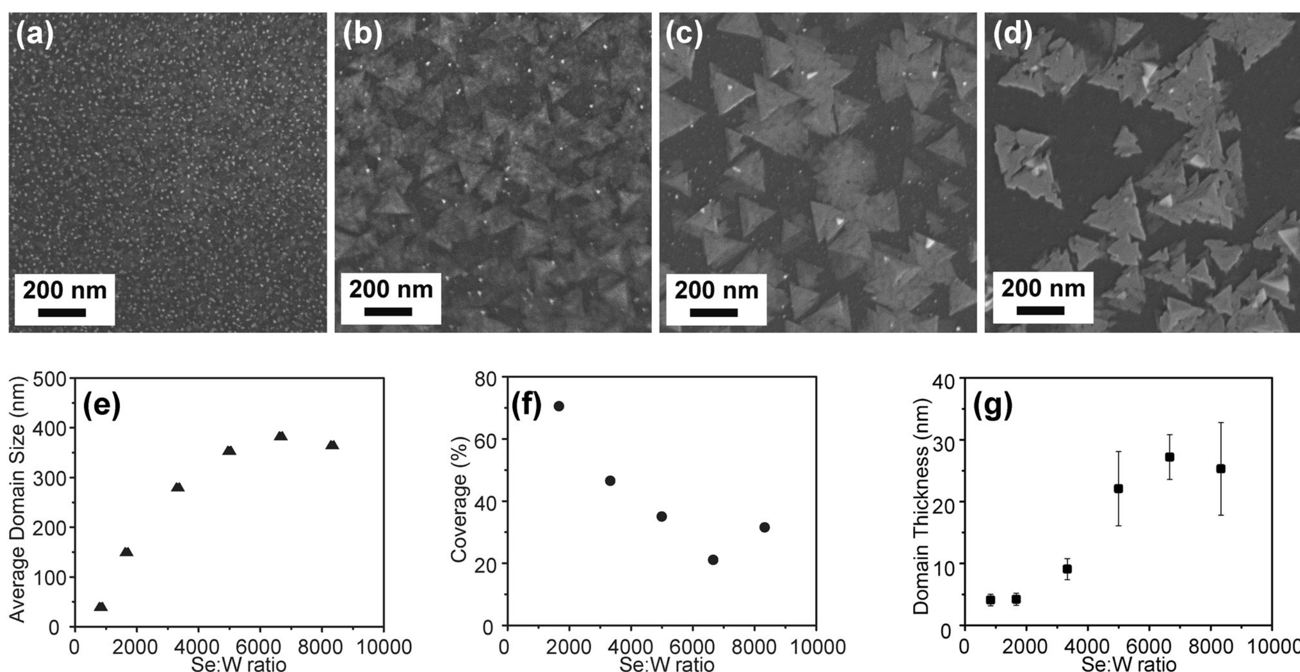

Fig. 1. FESEM images of WSe_2 domains grown on sapphire substrate using DMSe and $W(CO)_6$ as precursors with Se:W ratios of (a) 800, (b) 1600, (c) 3200, (d) 4800. The (e) average domain size, (f) surface coverage, and (g) domain thickness of the as-grown WSe_2 at Se:W ratios from 800 to 8000.

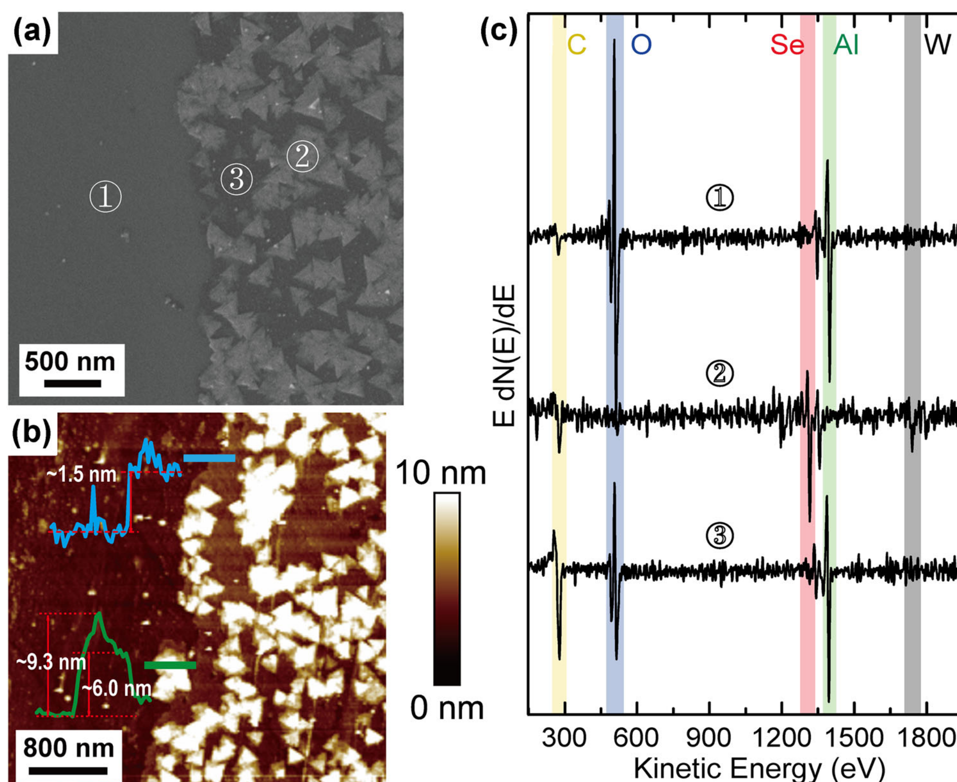

Fig. 2. (a) FESEM image of the WSe_2 sample grown at 800°C with Se:W = 3200 showing three regions: 1) sapphire surface; 2) WSe_2 triangular domains; 3) region of darker contrast between WSe_2 islands. (b) AFM image revealing a continuous layer ~1.5 nm thick and WSe_2 triangular domains ~6–9 nm thick on the sapphire surface. (c) AES spectra indicating the presence of Al and O in region 1, W, Se, and C in region 2, and Al, O, and C in region 3.

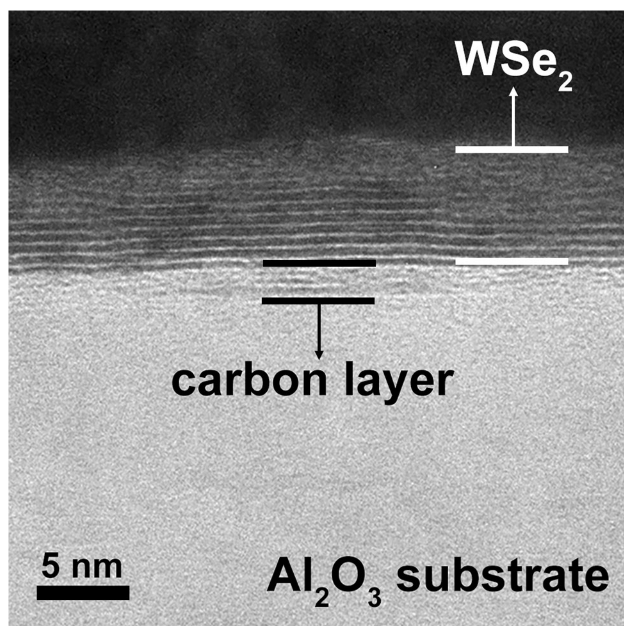

Fig. 3. Cross-sectional TEM image of WSe_2 sample grown using DMSe at 800°C and Se:W = 3200 revealing a carbon layer beneath the WSe_2. Some regions of the carbon layer exhibit a layered structure typical of defective graphene.

the DMSe precursor are likely responsible for the formation of the carbon layer on sapphire in the WSe_2 MOCVD process. Methyl radicals (CH_3*) are more chemically reactive than CH_4, consequently, this could lead to defective graphene formation at the lower temperatures (800°C) used in this study. Furthermore, the high Se:W ratios used in the growth result in an inlet C:W ratio, which is two times higher than the Se:W ratio creating a carbon-rich growth environment. To investigate this further, a growth run was carried out at 800°C under identical conditions to that used for WSe_2 growth but with only DMSe and H_2 flowing through the reactor. A high density of nanoscale nuclei were observed on the sapphire substrate through FESEM as shown in Fig. 4a. The Raman spectrum of this sample (Fig. 4b) revealed the presence of peaks associated with defective graphene. The presence of carbon G peak at ~1580 cm^{-1} and 2D peak at ~2680 cm^{-1} indicates a graphene-like structure,[25,27] while the high intensity of the carbon D peaks indicates that the graphene is highly defective.[25,26] The size of the defective graphene domains is small, less than 50 nm, possibly due to the low carbon adatom surface diffusion lengths and growth rate at

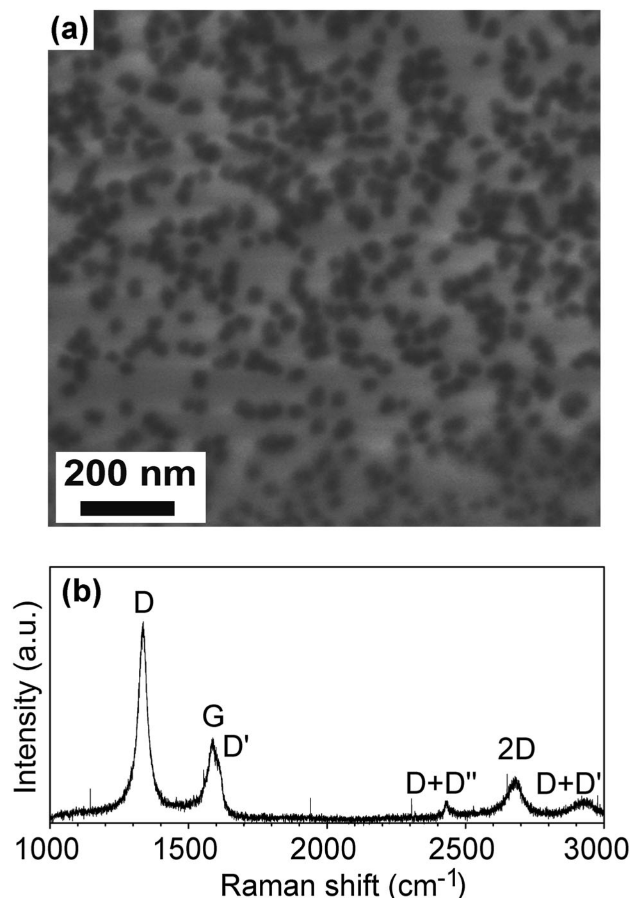

Fig. 4. Sapphire surface after flowing only DMSe and H_2 at 800°C under identical condition for WSe_2 growth: (a) FESEM image showing the presence of defective graphene domains; (b) Raman spectrum of sapphire surface showing G and 2D peaks associated with graphene and the family of D peaks indicating defects in the graphene.

800°C and the relatively short 30-min growth time. In contrast, the carbon layer in between the WSe_2 domains is continuous with a thickness of 1.5 nm suggesting that the deposition rate of carbon is higher in the presence of $W(CO)_6$. One interpretation is that the tungsten adatoms on the surface act as a catalyst to adsorb carbon and promote graphene formation as previously reported.[28]

Hydride precursors are typically utilized in III-V MOCVD to reduce carbon incorporation due to their lack of carbon-containing ligands and the atomic hydrogen produced from hydride decomposition which reacts with methyl groups on the surface to form methane that can readily desorb from substrate surface.[29,30] To investigate the effect of the chalcogen precursor chemistry, WSe_2 films were grown on sapphire using $W(CO)_6$ and H_2Se or DMSe using the same Se:W ratio of 3200 and substrate temperature of 800°C. Compared to the growth with DMSe (Fig. 5a), the Raman spectrum of the sample grown with H_2Se (Fig. 5b) shows negligible carbon D and G peaks, which indicates a significant reduction of carbon deposition on the sample. The AFM results also show significantly different nucleation density and lateral growth of WSe_2 with H_2Se versus DMSe. Unlike WSe_2 growth with DMSe where the surface coverage is reduced and the WSe_2 tends to grow vertically on top of existing WSe_2 islands instead of nucleating on the carbon-covered sapphire surface resulting in multi-layer domains ~10 nm in height, the density of WSe_2 domains is significantly increased with H_2Se resulting in a fully coalesced film, approximately 2 nm in thickness.

The defective graphene layer can also be viewed as a competitor to WSe_2 on the substrate surface and thus limits the nucleation as well as the lateral growth of WSe_2. As shown Fig. 1c and d, the WSe_2 nucleation density decreases but the domain size does not increase as the Se:W ratio is further increased from 3200 to 4800 and beyond. Increasing the Se:W results in a higher concentration of methyl radicals in the gas phase; therefore, more carbon atoms adsorb on the sapphire surface and occupy sites that would otherwise be available for nucleation and lateral growth of WSe_2. As a result, the W and Se atoms prefer to nucleate and grow on existing WSe_2 domains due possibly to site competition of W, Se, and C on the defective graphene surface and/or the reduced surface energy of the defective graphene compared to WSe_2. In either case, the presence of defective graphene on the sapphire surface increases the vertical-to-lateral growth of the WSe_2 domains. The results obtained for WSe_2 films grown with H_2Se, which contain negligible amounts of carbon support this interpretation. The absence of competing carbon adsorption, diffusion and graphene growth on the sapphire surface results in a higher nucleation density of WSe_2 and nearly complete coalescence of the films.

The results of this study demonstrate the potential problems that may be encountered in using organic chalcogen precursors in MOCVD growth of very thin TMDs films. MOCVD provides opportunities for scalability to large wafer sizes, improved thickness and composition uniformity and the ability for in situ heterostructure growth; however, carbon deposition as found in our experiments significantly reduces the ability of MOCVD to produce coalesced WSe_2 films with large domain sizes on sapphire substrates. It is also possible that carbon is incorporated substitutionally within the WSe_2 domains or is attached at the domain edge which could further impact the optical and electrical properties of the films, but additional studies are required to determine this. Also, carbon deposition is expected to be strongly dependent on the particular substrate used for MOCVD growth and may be less of a problem on amorphous surfaces such as SiO_2/Si, which do not typically promote graphene formation. In any event, hydride chalcogen precursors such as H_2Se are good candidates to replace organic chalcogen precursors used in growth although care must be taken when handling these sources due to their high toxicity.

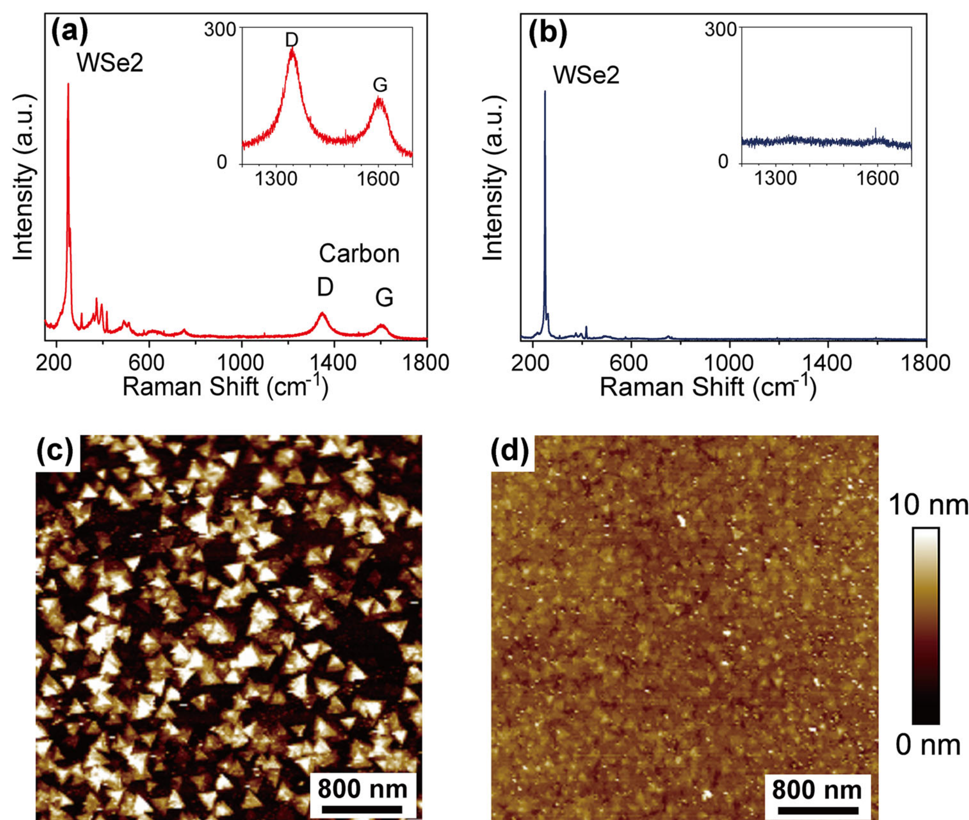

Fig. 5. Raman spectra of WSe_2 grown using (a) DMSe and (b) H_2Se at 800°C and Se:W ratio of 3200. The insets are zoom-in regions showing the carbon D and G peaks in WSe_2 grown with DMSe, but no carbon characteristic peaks in WSe_2 grown with H_2Se; and the AFM images of WSe_2 grown using (c) DMSe and (d) H_2Se.

CONCLUSION

A defective graphene layer was found to form simultaneously during MOCVD growth of WSe_2 on sapphire at high growth temperature and high Se:W ratios when using $W(CO)_6$ and DMSe as precursors. The formation of the defective graphene layer on sapphire competes with the nucleation and lateral growth of WSe_2 ultimately suppressing lateral growth and increasing the vertical growth rate of the domains. A coalesced few layer WSe_2 film was achieved using H_2Se instead of DMSe that eliminates the participation of methyl radicals in the growth environment and prevents the formation of defective graphene layer.

ACKNOWLEDGEMENTS

The authors acknowledge the financial support of The Dow Chemical Company and the National Science Foundation through EFRI 2-DARE Grant EFRI-1433378. This work was also supported in part by the Defense Threat Reduction Agency and the Center for Low Energy Systems Technology (LEAST), one of the six Semiconductor Research Corporation (SRC) Semiconductor Technology Advanced Research Network (STARnet) Centers, sponsored by the Microelectronics Advanced Research Corporation (MARCO) and the Defense Advanced Research Projects Agency (DARPA).

REFERENCES

1. K.F. Mak, C. Lee, J. Hone, J. Shan, and T.F. Heinz, *Phys. Rev. Lett.* 105, 136805 (2010).
2. H. Schmidt, F. Giustiniano, and G. Eda, *Chem. Soc. Rev. Chem. Soc. Rev* 44, 7715 (2015).
3. J.T. Ye, Y.J. Zhang, R. Akashi, M.S. Bahramy, R. Arita, and Y. Iwasa, *Science* 338, 1193 (2012).
4. S. Das, R. Gulotty, A.V. Sumant, and A. Roelofs, *Nano Lett.* 14, 2861 (2014).
5. D. Akinwande, N. Petrone, and J. Hone, *Nat. Commun.* 5, 5678 (2014).
6. R. Lv, J.A. Robinson, R.E. Schaak, D. Sun, Y. Sun, T.E. Mallouk, and M. Terrones, *Acc. Chem. Res.* 48, 56 (2015).
7. H. Hadouda, J. Pouzet, J.C. Bernede, and A. Barreau, *Mater. Chem. Phys.* 42, 291 (1995).
8. A. Khelil, H. Essaidi, J.C. Bernede, A. Bouacheria, and J. Pouzet, *J. Phys. Condens. Matter* 6, 8527 (1999).
9. Y. Lin, W. Zhang, J. Huang, K. Liu, Y. Lee, C. Liang, C. Chu, and L. Li, *Nanoscale* 4, 6637 (2012).
10. J.K. Huang, J. Pu, C.L. Hsu, M.H. Chiu, Z.Y. Juang, Y.H. Chang, W.H. Chang, Y. Iwasa, T. Takenobu, and L.J. Li, *ACS Nano* 8, 923 (2014).
11. K. Kang, S. Xie, L. Huang, Y. Han, P.Y. Huang, K.F. Mak, C.-J. Kim, D. Muller, and J. Park, *Nature* 520, 656 (2015).
12. S.M. Eichfeld, L. Hossain, Y. Lin, A.F. Piasecki, B. Kupp, A.G. Birdwell, R.A. Burke, N. Lu, X. Peng, J. Li, A. Azcatl, S. McDonnell, R.M. Wallace, M.J. Kim, T.S. Mayer, J.M. Redwing, and J.A. Robinson, *ACS Nano* 9, 2080 (2015).
13. N.D. Boscher, C.S. Blackman, C.J. Carmalt, I.P. Parkin, and A.G. Prieto, *Appl. Surf. Sci.* 253, 6041 (2007).
14. J.-W. Chung, Z.R. Dai, and F.S. Ohuchi, *J. Cryst. Growth* 186, 137 (1998).

15. N.D. Boscher, C.J. Carmalt, R.G. Palgrave, J.J. Gil-Tomas, and I.P. Parkin, *Chem. Vap. Depos.* 12, 692 (2006).
16. W. Hofmann, *J. Mater. Sci.* 23, 3981 (1988).
17. C.J. Carmalt, I.P. Parkin, and E.S. Peters, *Polyhedron* 22, 1499 (2003).
18. T.F. Kuech and J.M. Redwing, *J. Cryst. Growth* 145, 382 (1994).
19. S. Wang, Y. Rong, Y. Fan, M. Pacios, H. Bhaskaran, K. He, and J.H. Warner, *Chem. Mater.* 26, 6371 (2014).
20. S. Xie, M. Xu, T. Liang, G. Huang, S. Wang, G. Xue, N. Meng, Y. Xu, H. Chen, X. Ma, and D. Yang, *Nanoscale* 8, 219 (2015).
21. R. Ionescu, A. George, I. Ruiz, Z. Favors, Z. Mutlu, C. Liu, K. Ahmed, R. Wu, J.S. Jeong, L. Zavala, K.A. Mkhoyan, M. Ozkan, and C.S. Ozkan, *Chem. Commun.* 50, 11226 (2014).
22. K. Zhang, S. Feng, J. Wang, A. Azcatl, N. Lu, R. Addou, N. Wang, C. Zhou, J. Lerach, V. Bojan, M.J. Kim, L.Q. Chen, R.M. Wallace, M. Terrones, J. Zhu, and J.A. Robinson, *Nano Lett.* 15, 6586 (2015).
23. H.J. Song, M. Son, C. Park, H. Lim, M.P. Levendorf, A.W. Tsen, J. Park, and H.C. Choi, *Nanoscale* 4, 3050 (2012).
24. J. Hwang, M. Kim, D. Campbell, H.A. Alsalman, J.Y. Kwak, S. Shivaraman, A.R. Woll, A.K. Singh, R.G. Hennig, S. Gorantla, M.H. Rümmeli, and M.G. Spencer, *ACS Nano* 7, 385 (2012).
25. A.C. Ferrari and D.M. Basko, *Nat. Nanotechnol.* 8, 235 (2013).
26. M.A. Fanton, J.A. Robinson, C. Puls, Y. Liu, M.J. Hollander, B.E. Weiland, M. Labella, K. Trumbull, R. Kasarda, C. Howsare, J. Stitt, and D.W. Snyder, *ACS Nano* 5, 8062 (2011).
27. A.C. Ferrari, J.C. Meyer, V. Scardaci, C. Casiraghi, M. Lazzeri, F. Mauri, S. Piscanec, D. Jiang, K.S. Novoselov, S. Roth, and A.K. Geim, *Phys. Rev. Lett.* 97, 41 (2006).
28. W. Fang, A. Hsu, Y.C. Shin, A. Liao, S. Huang, Y. Song, X. Ling, M.S. Dresselhaus, T. Palacios, and J. Kong, *Nanoscale* 7, 4929 (2015).
29. R. Fornari, *Handbook of Crystal Growth: Thin Films and Epitaxy*, 2nd ed. (Waltham, MA; UK: Elsevier, 2014), pp. 1–49.
30. M.A. Malik and P. O'Brien, *Chemical Vapour Deposition: Precursors, Processes and Applications* (Cambridge: Royal Society of Chemistry, 2005), pp. 207–271.